Aeroelastic Tailoring Study of an N+2 Low-boom Supersonic Commercial Transport Aircraft

Chan-gi Pak[1]
NASA Armstrong Flight Research Center, Edwards, CA 93523-0273

The Lockheed Martin N+2 Low-boom Supersonic Commercial Transport (LSCT) aircraft was optimized in this study through the use of a multidisciplinary design optimization tool developed at the National Aeronautics and Space Administration Armstrong Flight Research Center. A total of 111 design variables were used in the first optimization run. Total structural weight was the objective function in this optimization run. Design requirements for strength, buckling, and flutter were selected as constraint functions during the first optimization run. The MSC Nastran code was used to obtain the modal, strength, and buckling characteristics. Flutter and trim analyses were based on ZAERO code, and landing and ground control loads were computed using an in-house code. The weight penalty to satisfy all the design requirements during the first optimization run was 31,367 lb, a 9.4% increase from the baseline configuration. The second optimization run was prepared and based on the big-bang big-crunch algorithm. Six composite ply angles for the second and fourth composite layers were selected as discrete design variables for the second optimization run. Composite ply angle changes can't improve the weight configuration of the N+2 LSCT aircraft. However, this second optimization run can create more tolerance for the active and near active strength constraint values for future weight optimization runs.

Nomenclature

AFRC = Armstrong Flight Research Center
AIL1 = aileron #1
AIL2 = aileron #2
BBBC = Big-Bang Big-Crunch
BF = body flap
BLF = buckling load factor
b = full span length
CG = center of gravity
C_p = pressure coefficient
c = chord length
DLW = design landing weight
DTOW = design take-off weight
DV_i = design variable i
d_{CG2MG} = distance from CG to main landing gear
d_{CG2NG} = distance from CG to nose landing gear
d_{NG2MG} = distance from nose landing gear to main landing gear
E = vertical height of the CG of the airplane above the ground in the 1.0 g static condition
EFEP = empty fuel empty payload
EFFP = empty fuel full payload
FE = finite element
FFEP = full fuel empty payload
FFFP = full fuel full payload
FM_{Lv} = Z component of the main landing gear load under a level landing condition

[1] Senior Aerospace Engineer, Aerostructures Branch, P.O. Box 273, Edwards, California/Mailstop 48201A, Senior Member AIAA.

FM_{St} = Z component of the main landing gear load under a static condition
FN_{Lv} = Z component of the nose landing gear load under a level landing condition
FN_{St} = Z component of the nose landing gear load under a static condition
FX = X component of load vector
FY = Y component of load vector
FZ = Z component of load vector
$F(\mathbf{X})$ = objective function
f = dynamic response factor; 2.0 is to be used unless a lower factor is substantiated
f_{LMG} = main landing gear ratio of level landing reactions to total weight of an aircraft
f_{LNG} = nose landing gear ratio of level landing reactions to total weight of an aircraft
GD = gear down (extended)
GU = gear up (retracted)
g = gravitational acceleration
$g_j(\mathbf{X})$ = inequality constraints (design requirements)
HSCT = high speed civil transport
L = left
LMSW = Lockheed Martin Skunk Works
LSCT = low-boom supersonic commercial transport
M2W = DTOW-fuel burned to reach Mach = 2
MDAO = multi-disciplinary analysis and optimization
MLG = main landing gear
MS = margin of safety
NASA = National Aeronautics and Space Administration
NLG = nose landing gear
Nx = acceleration in x-direction (fore and aft)
Nz = acceleration in z-direction (up and down)
ncon = number of constraints
ndv = number of design variables
O^3 = object-oriented optimization
P = roll rate
Pdot = roll acceleration
PI_B = performance index from the buckling post-processor module
PI_F = performance index from the flutter post-processor module
PI_S = performance index from the strength post-processor module
PI_W = performance index from the weight post-processor module
PLdB = perceived loudness in decibels
Post = post-processor module
Pre = pre-processor module
Q = pitch rate
Qdot = pitch acceleration
R = right
S = slope
SL = sea level
TEF = trailing-edge flap
V = velocity
V_e = equivalent speed
V-f = velocity versus frequency
V_F = flutter speed
V-g = velocity versus damping
V_L = limit speed
W_T = total weight
$\mathbf{X}$ = design variable vector, $\mathbf{X} = \lfloor X_{1,} X_{2,} \dots, X_n \rfloor^T$
X_i = i-th design variable
X_{CG} = X coordinate of the CG location
X_{MGCP} = X coordinate of the ground contact point of the main landing gear

X_{NGCP} = X coordinate of the ground contact point of the nose landing gear
Y_{CG} = Y coordinate of the CG location
Z_{CG} = Z coordinate of the CG location
Z_{MGCP} = Z coordinate of the ground contact point of the main landing gear
Z_{NGCP} = Z coordinate of the ground contact point of the nose landing gear
ZFW = zero fuel weight
α = angle of attack
μ = coefficient of friction
(CV) = constraints violated

I. Introduction

THE first supersonic flights of a commercial transport aircraft Tu-144 (Tupolev OKB, Moscow, Russia) and Concorde (British Aircraft Corporation, now British Aerospace, Westminster, London, United Kingdom) were in 1968 and 1969, respectively. The dream of flying from New York to Sydney in four hours hasn't been abandoned even with catastrophic failures leading to crashes of the Tu-144 and Concorde. The Tu-144 crashed during the Paris Air Show in 1973 and during delivery in 1978, and was then retired in 1983. At the Paris Air Show, the Tu-144 lost the left-hand (port) side of the whole wing during a descending maneuver. Concorde Air France Flight 4590 crashed during take-off in 2000 and the last Concorde flight was in 2003. Supersonic commercial transport aircraft designers are tasked to meet many requirements that include safety, sonic boom, and fuel efficiency issues. Outboard wing flutter and divergence associated with extensive outboard engine motion were one of the major issues during the design of High Speed Civil Transport (HSCT) aircraft[1,2] as shown in Fig. 1.

When an aircraft flies at supersonic speed, it creates a shock wave that imparts a thunder-like boom on the ground. To mitigate the unacceptable boom magnitudes, the United States and other countries limited supersonic routes of commercial transport aircraft to only those over the ocean. This sonic boom needs to be reduced drastically to enable supersonic commercial transport aircraft operation over the land.

The National Aeronautics and Space Administration (NASA) and the major private aerospace companies in the United States; The Boeing Company (Chicago, Illinois), Lockheed Martin (Bethesda, Maryland), Gulfstream Aerospace Corporation (Savannah, Georgia), and Aerion Corporation (Reno, Nevada); have continued to conduct research into Low-boom Supersonic Commercial Transport (LSCT) aircraft concepts to reduce the level of sonic boom on the ground within an acceptable range.[3-5] Lockheed Martin Skunk Works (LMSW) has developed an N+2 LSCT aircraft under a NASA contract.[4,5] The second next generation is referred as N+2. An artist concept of this aircraft is shown in Fig. 2. Cruise Mach number of 1.7 and a range of over 5,000 nautical miles were selected to design this 80-passenger aircraft.[5] This Lockheed Martin designed tri-jet aircraft achieved a sonic boom level of 79 PLdB at cruise speed. This sonic boom level was 6 dB, 20 dB, and 25 dB less than NASA's N+2 goal, HSCT aircraft, and Concorde, respectively.

Based on the current outer mold-line configuration, LMSW developed a detailed internal structural layout and delivered an aeroelastically optimized finite element (FE) model in gear-up (retracted) and gear-down (extended) configurations. The Lockheed Martin baseline FE model was sized using MSC Nastran (MSC Software Corporation, Newport Beach, California)[6] solution 200 (design optimization). One of the major difficulties in using MSC Nastran solution 200 for design optimization is that it is not easy to handle multiple structural models with multiple flight conditions in a single optimization run. In this study, the N+2 LSCT aircraft design at eight Mach numbers utilizes five and two fuel and payload conditions for landing gear-up and gear-down configurations, respectively. An object-oriented multidisciplinary design, analysis, and optimization (MDAO) tool[7] that has been developed at the NASA Armstrong Flight Research Center (AFRC) (Edwards, California) will be used to perform an aeroelastic tailoring study with multiple structural configurations and Mach numbers in a single optimization run.

The primary objective of the current aeroelastic tailoring study is to develop a baseline FE model for the Lockheed Martin N+2 LSCT aircraft. The long term objective of this design optimization study is using a game-changing approach for a light-weight aircraft design procedure. In this game-changing approach, flutter of an aircraft will be passively suppressed (i.e. use aeroelastic constraints) up to the limit speed line, and then actively suppressed between limit speed line and 15% limit speed margin line instead of using passive flutter suppression technique all the way up to 15% limit speed margin line as shown in Fig. 3. Therefore, simultaneous structural and control optimization[8,9] for reducing the structural weight using the aeroelastic tailoring and flexible motion control will be achieved in a single optimization run. Not only will the structural design variables, but also the control law design variables, such as coefficients of polynomials in the transfer functions et cetera, will be simultaneously changed during the optimization

to satisfy the open- and closed-loop flutter, gain and phase margin of the aeroservoelastic system, buckling, and overall strain requirements.

In the case of the current baseline optimization study, flutter of an aircraft will be suppressed all the way up to the 15% limit speed line. Therefore, results of the current baseline optimization study can be compared with the optimization results from the game-changing optimization study in the future.

The pre-matured version of a FE model delivered from LMSW in June 2013 was selected as a demonstration model in this study. The object-oriented MDAO tool is used in this study with structural behavior constraints, such as strength, buckling, and flutter. Structural analyses are based on MSC Nastran solution 103 (modal analysis) and 105 (buckling and strength analyses). The ZAERO code (Zona Technology Inc., Scottsdale, Arizona)[10] is used to obtain the aeroelastic characteristics of the N+2 LSCT aircraft in subsonic as well as supersonic speed regimes.

II. Object-Oriented Multidisciplinary Design, Analysis, and Optimization Tool

Supporting the Aeronautics Research Mission Directorate guidelines, NASA AFRC has developed an object-oriented optimization (O^3) tool[11] to leverage existing tools and practices, and to allow the easy integration and adoption of new state-of-the-art software.

Details of flow diagrams about pre-processor modules, discipline modules, and post-processor modules for flutter, buckling, and strength analyses used in this study are summarized in Fig. 4. These modules are script commands which mainly perform submission of the computing job, copying files, changing directories, saving files, and deleting files. Although these modules are developed mainly for MSC Nastran and ZAERO codes, they can be easily customized for other analytical tools. Some of these modules are discussed below.

A. Update Design Pre-processor Module (Pre: Update Design in Fig. 4)

This module reads in a template file for the MSC Nastran input deck, design variable data created by O^3 tool, and design variable to structural property relationship information, and then creates a new MSC Nastran input deck corresponding to the current design configuration. Design variables can be thicknesses and ply angles for composite plate/shell elements and area, area moment of inertia, and torsional constant for bar and beam elements, et cetera.

B. Modal Analysis Module (Discipline: Modal in Fig. 4)

MSC Nastran solution 103 (modal analysis) is used to determine the modal characteristics (natural frequencies and mode shapes), the global mass matrix, total weight, center of gravity (CG) locations, and mass moment of inertia of a structural model. Total weight, CG locations, and mass moment of inertia in the MSC Nastran output file (f06 file) are used in weight post-processor, update ZAERO pre-processor, and landing and ground control loads pre-processor modules. Natural frequencies and mode shapes are used for flutter and trim analyses and the global mass matrix is needed for trim analyses.

C. Weight Post-processor Module (Post: Weight in Fig. 4)

Two different weight computation modules were incorporated when the object-oriented MDAO tool was developed. The first module was based on the MSC Nastran output file (f06 file) from modal analysis. Total weight, CG locations, and mass moment of inertia are computed in this module. However, this module can be used only for light weight structural models due to the issue associated with the number of effective digits in the MSC Nastran output file. The second weight computation module was developed in this study to overcome this number of effective digits issue in the MSC Nastran output file. The second weight computation program reads in the MSC Nastran input deck and computes the total weight of a structural model.

In this study, weight computation is based on the design take-off weight (DTOW) condition. The DTOW is equivalent to full fuel full payload (FFFP) condition. Performance index from the weight post-processor module is the total weight as shown in Eq. (1):

$$\mathrm{PI_W} = W_T \tag{1}$$

D. Flutter Analysis and Flutter Post-processor Modules (Discipline: Flutter and Post: Flutter in Fig. 4)

The ZAERO code with g-method[10] solution technique and an in-house mode tracking code are used to determine the flutter speeds and frequencies. In the in-house mode tracking code, the flutter speeds are computed using the following definition together with the speed versus damping, V-g, and speed versus frequency, V-f, data obtained from ZAERO code. Definitions of flutter speed are illustrated in Fig. 5.

1) $V \leq V_L$: When speed is lower than a limit speed V_L, zero structural damping is assumed to compute flutter speed.
2) $V \geq 1.15V_L$: When speed is higher than $1.15V_L$, flutter speed computation is based on three percent structural damping.
3) $V_L < V < 1.15V_L$: When speed is between V_L and $1.15V_L$, linearly varying structural damping value is used to determine flutter speed.

In this study, a flutter speed V_F is designed to be higher than $1.15V_L$, as shown in Eq. (2):

$$V_F > 1.15V_L, \tag{2}$$

at a selected Mach number and altitude to have flutter free aircraft within flight envelope. Rewrite Eq. (2) as shown in Eq. (3):

$$1.15V_L - V_F < 0. \tag{3}$$

Dividing Eq. (3) by $1.15V_L$ gives the following design requirement shown in Eq. (4):

$$1 - \frac{V_F}{1.15V_L} < 0. \tag{4}$$

Therefore, the performance index from the flutter post-processor module is defined in Eq. (5):

$$PI_F \equiv 1 - \frac{V_F}{1.15V_L} \tag{5}$$

where, V_F is the flutter speed obtained from the post-processor module.

E. Update ZAERO Pre-processor, Trim Analysis, and Trim Loads Pre-processor Modules (Pre: Update ZAERO, Discipline: Trim, and Pre: Trim Loads in Fig. 4)

The ZAERO trim analysis is used to compute a design load (inertia load + aerodynamic load) for various design configurations. During optimization, an input deck for ZAERO trim analysis is updated in the update ZAERO pre-processor module using total weight, CG locations, moment of inertias, and the global mass matrix computed from the modal analysis module.

Sometimes, computed design loads are not symmetric from symmetric trim analysis due to the numerical difficulties associated with a splining procedure. In this study, the trim loads pre-processor module reads in external loads computed from the trim analysis module, generates symmetric or anti-symmetric loads, and writes manipulated design loads for strength and buckling analyses. Trim flight conditions used in this study are summarized in Table 1.

F. Landing and Ground Control Loads Pre-processor Module (Pre: Landing & Ground Loads in Fig. 4)

This pre-processor module computes landing, ground control, and emergency landing loads.[12] Landing conditions used in the design procedure are as follows:

- Level landing
- Spin up landing
- Spring back landing
- Lateral drift landing
- Right gear landing
- Left gear landing
- Side load right (R) to left (L)
- Side load L to R

Ground control loads are computed using the following conditions:

- Three-point braking roll
- Two-points braking roll
- Dynamic roll braking
- Turning condition
- Nose wheel yaw and steering 1
- Nose wheel yaw and steering 2

- Nose wheel yaw and steering 3
- Reverse braking
- 2g taxi

Finally, emergency landing loads applied to three engine structures are computed based on the following conditions:

- 9g forward loading
- 1.5g rearward loading
- 3g sideway loading
- 6g downward loading

Landing and ground control loads computations are based on equations in Tables 2 and 3, respectively.

G. Buckling and Strength Analyses and Strength Post-processor Modules (Discipline: Buckling and Strength and Post: Strength in Fig. 4)

Based on design loads computed from trim, landing (regular as well as emergency), and ground control analyses, strength and buckling analyses are performed simultaneously using MSC Nastran solution 105. Once a landing gear configuration and a weight condition are selected then all kinds of different load subcases can be analyzed in a single MSC Nastran solution 105.

For the static safety of a structure, design load multiplied by safety factor applied to a structural element should be smaller than a corresponding failure load as shown in Eq. (6):

$$\text{Design Load} \times \text{Safety Factor} < \text{Failure Load}. \tag{6}$$

Rearranging above equation gives Eq. (7):

$$\text{Design Load} \times \text{Safety Factor} - \text{Failure Load} < 0. \tag{7}$$

Dividing Eq. (7) by "Design Load $\times$ Safety Factor" gives Eq. (8):

$$1 - \frac{\text{Failure Load}}{\text{Design Load} \times \text{Safety Factor}} < 0. \tag{8}$$

Margin of safety (MS) is defined in Eq. (9):

$$\text{MS} \equiv \frac{\text{Failure Load}}{\text{Design Load} \times \text{Safety Factor}} - 1. \tag{9}$$

The minimum margin of safety from all of the structural elements under all of the different load subcases is selected as the performance index from strength post-processor. Therefore, one performance index, that is critical MS, is obtained from one MSC Nastran solution 105 run as shown in Eq. (10):

$$\text{PI}_s \equiv -\min(\text{MS}) \tag{10}$$

A safety factor of 1.5 is used for all metal and composite materials in this study.

H. Buckling Post-processor Module (Post: Buckling in Fig. 4)

The buckling load factor (BLF) is the factor of safety against buckling phenomena and possible BLF values with corresponding buckling status are summarized as follows:

- $0 \leq \text{BLF} \leq 1$: Buckling predicted
- $\text{BLF} < 0$ or $\text{BLF} > 1$: Buckling not predicted

Therefore, buckling will be predicted when the BLF value is within the following ranges in Eq. (11):

$$0 \leq \text{BLF} \leq 1 \tag{11}$$

Subtracting $1/2$ from Eq. (11) gives Eq. (12):

$$-1/2 \leq \text{BLF} - 1/2 \leq 1/2 \tag{12}$$

Eq. (12) is equal to Eq. (13):

$$(\mathrm{BLF} - 1/2)^2 \leq (1/2)^2 \tag{13}$$

Therefore, if the opposite description in Eq. (14) is true,

$$(\mathrm{BLF} - 1/2)^2 > (1/2)^2, \tag{14}$$

then buckling is not predicted. Rewrite Eq. (14), as shown in Eq. (15):

$$(1/2)^2 - (\mathrm{BLF} - 1/2)^2 < 0. \tag{15}$$

A performance index from buckling post-processor is defined using the positive minimum BLF value from all of the different load subcases, and computed from Eq. (16).

$$\mathrm{PI_B} \equiv (1/2)^2 - \{\text{positive min}(\mathrm{BLF}) - 1/2\}^2 \tag{16}$$

III. Multidisciplinary Analysis of the Aircraft Model before Optimization

In this section, modal, flutter, trim, landing and ground control, strength, and buckling analyses have been performed before starting optimization in order to have reference structural characteristics of the N+2 LSCT aircraft. The MSC Nastran code is used to obtain the modal, strength, and buckling characteristics. Flutter and trim analyses are based on ZAERO code, and landing and ground control loads are computed using an in-house code.

A. Modal Analysis

A structural FE model with gear-down configuration is shown in Fig. 6. The total number of grid points in the gear-up FE model is 55,635, and the total weight in the DTOW condition is 332,738 lbf.

Fifty and sixteen modes are computed for the flutter and trim analyses, respectively. Natural frequencies for the first ten elastic modes from gear-up with DTOW, full fuel empty payload (FFEP), DTOW minus fuel burned to reach Mach 2 weight (M2W), and zero fuel weight (ZFW) configurations; and gear-down with DTOW and design landing weight (DLW = ZFW+35% Fuel) configurations are summarized in Table 4. The ZFW is equivalent to empty fuel full payload (EFFP) condition. The first six flexible mode shapes obtained from gear-up with DTOW configuration are shown in Fig. 7.

B. Flutter Analysis

The aerodynamic model of the N+2 LSCT aircraft based on ZAERO computation is shown in Fig. 8. This ZAERO aerodynamic model has 5,060 surface elements. The matched flutter analyses are performed at six Mach numbers of 0.66, 0.89, 1.41, 1.80, 2.00, and 2.30 using DTOW, FFEP, empty fuel empty payload (EFEP), and ZFW conditions. The velocity versus damping, V-g, and velocity versus frequency, V-f, curves of the baseline model with the DTOW condition at a Mach number of 0.66 from the matched flutter analyses are given in Fig. 9. The primary flutter mode shape using DTOW condition at Mach 0.66 is given in Fig. 10. In this flutter mode shape, the outboard wing and V-tail are coupled through the flexibility of the aft inner wing section, and the center engine pitch motion is also involved in this first flutter mode shape. Flutter boundaries before optimization are summarized in Fig. 11. It should be noted in Fig. 11 that the fuel effect on flutter boundaries are larger than the payload effect. Flutter speeds at Mach 0.66 and 0.89 for full fuel conditions DTOW and FFEP are between V_L and $1.15V_L$. Therefore, flutter design requirements are violated at these two Mach numbers with full fuel conditions.

C. Trim Analysis

The control surfaces for trim analyses are displayed in Fig. 12. Trim analyses are also performed using the ZAERO code, and trim results are given in the appendix. Symmetric trim analyses are performed using the gear-up configuration with DTOW, ZFW, and M2W conditions; and gear-down configuration with DTOW and DLW conditions. Anti-symmetric trim analyses are also performed in the case of the gear-up configuration with the DTOW condition.

The ZAERO based aerodynamic model gives more realistic aerodynamic loads on the fuselage area compared to the MSC Nastran model (using the doublet lattice method) in reference 5. In this reference, the accuracy of the design aerodynamic load on the fuselage area was questionable since the fuselage of the N+2 LSCT aircraft had been

idealized using flat horizontal panels instead of using three dimensional body type elements as shown in Fig. 8. Especially, since there are no applied horizontal design aerodynamic loads for the fuselage design in reference 5.

D. Landing and Ground Control Analyses

Landing and ground control load vectors for twenty one load cases with DTOW and DLW conditions are computed in this study. Eight, nine, and four load cases as given in section II-F are from landing, ground control, and emergency landing conditions, respectively. In the case of landing analysis, trimmed aerodynamic loads from load cases 1500 and 1800 are added for weight conditions DTOW and DLW, respectively.

E. Buckling and Strength Analyses

In this study, buckling and strength analyses are performed simultaneously using MSC Nastran solution 105. A total number of five buckling and strength analyses with gear-up (three analyses) and gear-down (two analyses) configurations are performed. These five different structural models are summarized in Table 5. Minimum buckling load factors before optimization from each analysis set are summarized in Table 6, and a buckling mode shape under the gear-up and DTOW condition is shown in Fig. 13. The gear-up configuration of the N+2 LSCT aircraft has buckling issues as shown in Table 6. On the other hand, the gear-down configuration is buckling free.

Minimum margin of safety values of the N+2 LSCT aircraft before optimization from five MSC Nastran solution 105 are summarized in Table 7. Negative margin of safety values are observed for all five different sets of the model, and that means strength design requirements are all violated with the ZAERO based aerodynamic model. Violation of margin of safety values probably means that the aerodynamic loads distribution computed using ZAERO trim analysis are different than the MSC Nastran generated aerodynamic loads.[5]

IV. Multidisciplinary Design Optimization

In this study, the optimization problem is stated as follows:

Find design variables $\mathbf{X} = \left\lfloor X_{1,} X_{2,} \dots, X_n \right\rfloor^T$ which minimizes Eq. (17):

$$F(\mathbf{X}) \qquad \text{objective function} \tag{17}$$

subjected to Eqs. (18) and (19):

$$g_j(\mathbf{X}) < 0. \qquad j = 1,2, \dots, ncon \qquad \text{inequality constraints} \tag{18}$$

$$X_i^L \le X_i \le X_i^U \;\; i = 1,2, \dots, ndv \qquad \text{side constraints} \tag{19}$$

Based on the analyses before optimization in section III, most of the flutter, buckling, and strength design requirements are violated under ZAERO based aerodynamics as shown in Table 8. The fuselage aerodynamic model is better with the ZAERO model, shown in Fig. 8, than the MSC Nastran based model.[5] The ZAERO based aerodynamic loads are larger than MSC Nastran based loads, and therefore most of the design requirements are violated as shown in Table 8 under the before optimization column.

A. First Optimization Run (Sizing Optimization)

One of the major issues with the gradient based optimization algorithms such as Automated Design Synthesis[13] (ADS) or Design Optimization Tools[14] (DOT) is that the starting configuration of an optimization run should be in the feasible domain. Otherwise, there is no guarantee that the optimizer program will eventually push the design from an infeasible domain to a feasible domain. In this study, composite ply thicknesses of the failed finite elements are manually stiffened to have a feasible design. A total number of 111 variables are selected and thickened to have a feasible design at a starting configuration. Objective function value and corresponding constraint function values at a starting configuration are also given in Table 8 under the iteration 1 column. The weight penalty for having an achievable (or feasible) design was 93,026 lb (a 28.0% increase from baseline).

These 111 variables are selected as design variables for the first optimization run. Structural components affected by these 111 design variables are shown in Fig. 14 using colored elements. In the baseline model, composite materials are based on the stacking of the nine plies, and cross sectional configuration is shown in Fig. 15. Design variable linking is defined based on the different structural components and summarized as follows:

- Wing, inner-wing, tail, and fuselage skins; three design variables per each composite laminate property
  - 1st ply thickness, 2nd ply thickness = 4th ply thickness, and 3rd ply thickness

- Spars and ribs for wing, inner-wing, and tail as well as bulkheads and walls for fuselage; one design variable per each composite laminate property
    - 1st ply thickness = 2nd ply thickness = 3rd ply thickness = 4th ply thickness
- Spars and ribs for inner-wing; one design variable per each composite laminate property
    - 5th ply thickness

Objective as well as constraint functions and corresponding performance indices for the first optimization run are summarized in Table 9. After the first seven iterations, structural weight of the DTOW condition is reduced, and all the constraint functions $g_j(\mathbf{X})$ satisfy required values, i.e. $g_j(\mathbf{X}) < 0$. $j = 1,2,\ldots,16$. The weight reduction was 61,659 lb, and therefore, weight penalty at the end of the first optimization run is 31,367 lb (a 9.4% increase from baseline). Change of the composite ply thickness design variables after iteration 7 are shown in Fig. 16. In this figure, color spectrums represent "composite laminate thickness after optimization" divided by "composite laminate thickness before optimization".

The active and near active strength constraints at the end of the first optimization run are from buckling and strength analyses set number 4, 2, and 1 as shown in Table 8 under the iteration 7 column. Corresponding weight and gear configurations are gear up with DTOW and ZFW conditions and gear down with the DTOW condition. Strain distributions under these active and near active strength constraints are shown in Fig. 17.

The active constraint is from load case number 3013, and this case corresponds to nose wheel yaw and steering case number 1 as shown in Tables 3 and 5. The margin of safety value before optimization was -0.781 as shown in Table 7. This margin of safety value becomes 5.36e-6 (effectively zero) after the first optimization run. The active element is located at the second rib of the inner wing near the main landing gear bay area as shown in Fig. 17a.

Two near active strength constraints are load case numbers 1700 and 300 from the gear up with ZFW and DTOW conditions, respectively. These cases match with 2.7g gust and 2.5g pull up maneuver loading cases under Mach numbers of 0.89 and 0.48, respectively, as shown in Table 1. Strain distributions are shown in Figs. 17b and 17c. In these figures, active elements are located at the floor of the main landing gear bay. The margin of safety value for load case 1700 was -0.998 before optimization and becomes 0.061 after the first optimization run. On the other hand, load case 1400 for the near active strength constraint in Table 7 is switched to load case 300 after the first optimization run, and the margin of safety value is changed from -0.999 to 0.161.

The near active flutter constraints are from DTOW and FFEP weight conditions at Mach 0.89. The only area in the wing affected by design variables is near the trailing-edge of the wing tip section as shown in Fig. 14. By doubling the total thickness of this area, flutter boundaries are outside 1.15 V_L line. Adding weight near the trailing-edge of the wing tip section is a kind of mass balancing effect on flutter boundaries which can be observed in reference 7.

B. Second Optimization Run (Aeroelastic Tailoring Optimization)

Six design variables are selected for the second optimization run. From the active strength constraint case, the design variable for the active element area in Fig. 17a was the composite core thickness, and therefore, angles for the second and fourth plies in the area of zone 1 in Fig. 18 are selected as the first design variable for the second optimization. Right and left hand side as well as upper and lower ply angle design variables are linked in this study.

The second design variable is selected from zone 2 in Fig. 18. From the near active strength constraint, the active elements in Figs 17b and 17c are located at the floor of the main landing gear bay (near the junction of the floor and centerline wall). However, composite laminate thicknesses in this area were between 6 to 10 times thicker than the starting configuration as shown in Fig. 16, and therefore, angles for the second and fourth plies are selected as the second design variable, which are also linked, the same as the first design variable.

The third and fourth design variables are also selected near the main landing gear bay area as shown in Fig. 18, zone 3 and zone 4. As shown in Fig. 16, composite laminate thicknesses in these areas were between 2 to 6 times thicker compared to the starting configuration, and these two zones are connected to the floor of the main landing gear bay. Therefore angles for the second and fourth plies for zones 3 and 4 are also selected as design variables.

Finally, the fifth and sixth design variables are angles for the second and fourth plies for zone 5 and zone 6 in the aft fuselage skin area as shown in Fig. 18. In Fig. 16, composite laminate thicknesses changes in these two zones are almost 3 to 16 times thicker than the starting configuration, and therefore, design variables are selected in these two zones.

Objective and constraint functions for the second optimization run are also summarized in Table 9. Composite ply angle change cannot improve weight configuration. Therefore, the active and the near active strength constraint values; minimum margin of safety values from three strength analyses set numbers 1, 2, and 4; will be maximized to create more tolerance, as defined in Fig. 19 for the future weight optimization runs. Therefore, the linear combination of these three margin of safety values becomes the objective function for the second optimization run. Weighting factors for these three performance indices, $g_{15}(\mathbf{X})$, $g_{13}(\mathbf{X})$, and $g_{12}(\mathbf{X})$, for the objective function are 1.0, 0.5, and 0.5,

respectively. Constraint functions for the second optimization run are the same as the first optimization run, and therefore performance indices $g_{15}(\mathbf{X})$, $g_{13}(\mathbf{X})$, and $g_{12}(\mathbf{X})$ are both in objective and constraint functions.

Discrete variables are used for ply angles which are discretized every 5° from 0° to 90°. These design variables are related to the $\pm 45°$ ply angles shown in Fig. 15; the second, fourth, sixth, and eighth plies. Plus 45° and minus 45°angles are also linked to reduce the total number of design variables for the second optimization run.

Discrete design variables together with the big-bang big-crunch (BBBC) algorithm[15-18] are used in the second optimization run. Number of populations and BBBCs are 60 and 2, respectively. Objective as well as constraint functions and discrete design variable histories are given in Tables 10 and 11, respectively. In Table 10, the active and two near active strength constraint values of -5.63e-6, -0.061, and -0.161 become -0.159, -0.145, and -0.232, respectively. Therefore, the second optimization run creates more tolerance values from constraint boundaries for future weight optimization runs.

V. Conclusion

The Lockheed Martin pre-matured N+2 LSCT aircraft is optimized in this study through the use of a multidisciplinary design optimization tool developed at the NASA AFRC. The baseline design of the pre-matured N+2 LSCT aircraft was infeasible when ZAERO based aeroelastic analyses were used. Most of the flutter, buckling, and strength design requirements were violated, and therefore, the composite thickness variables were changed manually to have a feasible starting configuration. The starting configuration of the optimization run should be an achievable design, and the weight penalty for this was 93,026 lb (a 28.0% increase from baseline).

A total of 111 design variables are used in the first optimization run. During the first optimization run, the weight reduction was 61,659 lb, and therefore, the weight penalty at the end of the first optimization run is 31,367 lb (a 9.4% increase from baseline). All the design requirements of the N+2 LSCT aircraft are satisfied at the end of the first optimization run. The active strength constraint at the end of the first optimization run was under the nose wheel yaw and steering case number 1. The minimum margin of safety under this load condition was 5.36e-6, effectively zero. This minimum value is associated with the structural component located at the second rib of the inner wing near the main landing gear bay area. Two near active constraints are also due to the strength requirement. Minimum margin of safety values of 0.061 and 0.161 are observed at the floor of the main landing gear bay area. Corresponding load cases are the 2.7g gust load case at Mach 0.89 and an altitude of 20,000 ft and a 2.5g maneuver load case at sea level under Mach 0.48. The near active flutter constraint is related to the flutter boundary requirement at Mach number of 0.89 under DTOW and FFEP load conditions, and the design was improved due to the mass balancing effect.

The second optimization run is prepared and based on the six discrete design variables with the BBBC algorithm. Angles for the second and fourth plies are selected as discrete design variables for the second optimization runs. Ply angle changes cannot improve the weight configuration of the N+2 LSCT aircraft. However, strength properties can be changed with different ply angles. Therefore, the second optimization run can create more tolerance for the active as well as near active strength constraint values for future weight optimization runs.

Tables

Table 1. Trim flight conditions.

Load case ID	Maneuver	Load factor	Mach number	Weight	Landing gear	Altitude	Trim variables
100	Pull up	2.5g	0.66	DTOW	Up	SL	BF(R=L)
200	Push over	-1g	0.66	DTOW	Up	SL	BF(R=L)
300	Pull up	2.5g	0.48	DTOW	Up	SL	BF(R=L)
400	Pull up	2.5g	2.00	M2W	Up	49,770ft	BF=TEF(R=L)
500	Push over	-1g	2.00	M2W	Up	49,770ft	BF(R=L)
600	Pull up	2.5g	1.41	DTOW	Up	49,770ft	BF=TEF=AIL1=AIL2(R=L)
700	Pull up	2.5g	0.66	ZFW	Up	SL	BF(R=L)
800	Push over	-1g	0.66	ZFW	Up	SL	BF(R=L)
900	Pull up	2.5g	2.00	ZFW	Up	49,770ft	BF=TEF(R=L)
1000	Push over	-1g	2.00	ZFW	Up	49,770ft	BF(R=L)
1100	Steady roll	0g	0.48	DTOW	Up	SL	Load Case 2100+2300
1200	Abrupt roll	0g	0.48	DTOW	Up	SL	Load Case 2200+2300
1300	Steady roll	1.67g	0.48	DTOW	Up	SL	Load Case 2100+2400
1400	Abrupt roll	1.67g	0.48	DTOW	Up	SL	Load Case 2200+2400
1500	Landing	1g	0.3092	DTOW	Down	SL	BF(R=L)
1600	Cruise	1g	1.80	DTOW	Up	55,000ft	BF=TEF(R=L)
1700	Gust loads	2.7g	0.89	ZFW	Up	20,000ft	BF(R=L)
1800	Landing	1g	0.3092	DLW	Down	SL	BF(R=L)
2100	Steady roll	0g	0.48	DTOW	Up	SL	AIL1=AIL2(R=-L)
2200	Abrupt roll	0g	0.48	DTOW	Up	SL	AIL1=AIL2(R=-L)
2300	Pull up	0g	0.48	DTOW	Up	SL	BF(R=L)
2400	Pull up	1.67g	0.48	DTOW	Up	SL	BF(R=L)

Table 2. Equations for landing load computations.

Load cases	Case number	Load	Right-MLG	Left-MLG	NLG
Level + trim load	3001 (DTOW) & 4001 (DLW)	FX	$0.25\mathrm{FM}_{Lv}$	$0.25\mathrm{FM}_{Lv}$	$0.25\mathrm{FN}_{Lv}$
		FY	0.0	0.0	0.0
		FZ	$\mathrm{FM}_{Lv} = \mathrm{f}_{LMG}\mathrm{W}_T$	FM_{Lv}	$\mathrm{FN}_{Lv} = \mathrm{f}_{LNG}\mathrm{W}_T$
Spin up + trim load	3002 (DTOW) & 4002 (DLW)	FX	$(0.8 \times 0.8)\mathrm{FM}_{Lv}$	$(0.8 \times 0.8)\mathrm{FM}_{Lv}$	$(0.8 \times 0.8)\mathrm{FN}_{Lv}$
		FY	0.0	0.0	0.0
		FZ	$0.8\mathrm{FM}_{Lv}$	$0.8\mathrm{FM}_{Lv}$	$0.8\mathrm{FN}_{Lv}$
Spring back + trim load	3003 (DTOW) & 4003 (DLW)	FX	$-(0.8 \times 0.8)\mathrm{FM}_{Lv}$	$-(0.8 \times 0.8)\mathrm{FM}_{Lv}$	$-(0.8 \times 0.8)\mathrm{FN}_{Lv}$
		FY	0.0	0.0	0.0
		FZ	$0.8\mathrm{FM}_{Lv}$	$0.8\mathrm{FM}_{Lv}$	$0.8\mathrm{FN}_{Lv}$
Lateral drift + trim load	3004 (DTOW) & 4004 (DLW)	FX	$(0.4 \times 0.75)\mathrm{FM}_{Lv}$	$(0.4 \times 0.75)\mathrm{FM}_{Lv}$	$0.4\mathrm{FN}_{Lv}$
		FY	$(0.25 \times 0.75)\mathrm{FM}_{Lv}$	$(0.25 \times 0.75)\mathrm{FM}_{Lv}$	$0.25\mathrm{FN}_{Lv}$
		FZ	$0.75\mathrm{FM}_{Lv}$	$0.75\mathrm{FM}_{Lv}$	FN_{Lv}
Right one gear + trim load	3005 (DTOW) & 4005 (DLW)	FX	$0.25\mathrm{FM}_{Lv}$	0.0	0.0
		FY	0.0	0.0	0.0
		FZ	FM_{Lv}	0.0	0.0
Left one gear + trim load	3006 (DTOW) & 4006 (DLW)	FX	0.0	$0.25\mathrm{FM}_{Lv}$	0.0
		FY	0.0	0.0	0.0
		FZ	0.0	FM_{Lv}	0.0
Side load RtoL + trim load	3007 (DTOW) & 4007 (DLW)	FX	0.0	0.0	0.0
		FY	$(0.8 \times 0.5)\mathrm{FM}_{Lv}$	$(0.6 \times 0.5)\mathrm{FM}_{Lv}$	0.0
		FZ	$0.5\mathrm{FM}_{Lv}$	$0.5\mathrm{FM}_{Lv}$	0.0
Side load LtoR + trim load	3008 (DTOW) & 4008 (DLW)	FX	0.0	0.0	0.0
		FY	$-(0.6 \times 0.5)\mathrm{FM}_{Lv}$	$-(0.8 \times 0.5)\mathrm{FM}_{Lv}$	0.0
		FZ	$0.5\mathrm{FM}_{Lv}$	$0.5\mathrm{FM}_{Lv}$	0.0
DTOW		f_{LMG}=0.36; f_{LNG}=0.0639; Trim load case ID = 1500			
DLW		f_{LMG}=1.20; f_{LNG}=0.1477; Trim load case ID = 1800			

Table 3. Equations for ground control load computations.

Load cases	Case number	Load	Right-MLG	Left-MLG	NLG
Static condition		FX	0.0	0.0	0.0
		FY	0.0	0.0	0.0
		FZ	$\mathrm{FM}_{St} = \frac{0.5\mathrm{d}_{CG2NG}\mathrm{W}_T}{\mathrm{d}_{NG2MG}}$	FM_{St}	$\mathrm{FN}_{St} = \frac{\mathrm{d}_{CG2MG}\mathrm{W}_T}{\mathrm{d}_{NG2MG}}$
3-point braked roll	3009 (DTOW) & 4009 (DLW)	FX	$0.8\mathrm{FM}_{St}$	$0.8\mathrm{FM}_{St}$	0.0
		FY	0.0	0.0	0.0
		FZ	FM_{St}	FM_{St}	$\frac{2\mathrm{d}_{CG2MG}\mathrm{FM}_{St} + 2(Z_{CG} - Z_{MGCP})0.8\mathrm{FM}_{St}}{\mathrm{d}_{CG2NG}}$
2-point braked roll	3010 (DTOW) & 4010 (DLW)	FX	$0.8\mathrm{FM}_{St}$	$0.8\mathrm{FM}_{St}$	0.0
		FY	0.0	0.0	0.0
		FZ	FM_{St}	FM_{St}	0.0
Dynamic roll braking	3011 (DTOW) & 4011 (DLW)	FX	$0.8\mathrm{FM}_{St}$	$0.8\mathrm{FM}_{St}$	0.0
		FY	0.0	0.0	0.0
		FZ	FM_{St}	FM_{St}	$\frac{\mathrm{W}_T}{\mathrm{d}_{NG2MG}}\left[\mathrm{d}_{CG2MG} + \frac{\mathrm{fd}_{CG2NG}\mu E}{\mathrm{d}_{NG2MG} + \mu E}\right]$ where, $E = \{Z_{CG} - Z_{NGCP} - (X_{CG} - X_{NGCP})S\}$ and $S = (X_{CG} - X_{NGCP})\frac{Z_{MGCP} - Z_{NGCP}}{X_{MGCP} - X_{NGCP}}$
Turning Condition	3012 (DTOW) & 4012 (DLW)	FX	0.0	0.0	$0.25\mathrm{FN}_{St}$
		FY	$0.5\mathrm{FM}_{St}$	$0.5\mathrm{FM}_{St}$	$0.5\mathrm{FN}_{St}$
		FZ	FM_{St}	FM_{St}	FN_{St}
Nose wheel yaw and steering (1)	3013 (DTOW) & 4013 (DLW)	FX	0.0	0.0	0.0
		FY	0.0	0.0	$0.8\mathrm{FN}_{St}$
		FZ	FM_{St}	FM_{St}	FN_{St}
Nose wheel yaw and steering (2)	3014 (DTOW) & 4014 (DLW)	FX	$0.8\mathrm{FM}_{St}$	0.0	0.0
		FY	0.0	0.0	0.0
		FZ	FM_{St}	FM_{St}	$\frac{2\mathrm{d}_{CG2MG}\mathrm{FM}_{St} + (Z_{CG} - Z_{MGCP})0.8\mathrm{FM}_{St}}{\mathrm{d}_{CG2NG}}$
Nose wheel yaw & steering (3)	3015 (DTOW) & 4015 (DLW)	FX	0.0	$0.8\mathrm{FM}_{St}$	0.0
		FY	0.0	0.0	0.0
		FZ	FM_{St}	FM_{St}	$\frac{2\mathrm{d}_{CG2MG}\mathrm{FM}_{St} + (Z_{CG} - Z_{MGCP})0.8\mathrm{FM}_{St}}{\mathrm{d}_{CG2NG}}$
Reversed braking	3016 (DTOW) & 4016 (DLW)	FX	$-0.55\mathrm{FM}_{St}$	$-0.55\mathrm{FM}_{St}$	0.0
		FY	0.0	0.0	0.0
		FZ	FM_{St}	FM_{St}	0.0
2G taxi	3017 (DTOW) & 4017 (DLW)	FX	0.0	0.0	0.0
		FY	0.0	0.0	0.0
		FZ	$2\mathrm{FM}_{St}$	$2\mathrm{FM}_{St}$	$2\mathrm{FN}_{St}$
$\mu = 0.80$; f = 2.00 $\mathrm{d}_{NG2MG} \equiv \mathrm{d}_{CG2NG} + \mathrm{d}_{CG2MG}$					

Table 4. Natural frequencies of the N+2 LSCT aircraft with different fuel and payload conditions before optimization.

Mode number	Natural frequency (Hz)						Notes
	Gear-up				Gear-down		
	DTOW	FFEP	M2W	ZFW	DTOW	DLW	
7	2.049	2.055	2.071	2.266	2.048	2.158	Aft fuselage torsion
8	2.235	2.262	2.277	2.554	2.238	2.424	First symmetric fuselage bending
9	2.498	2.509	2.539	2.993	2.503	2.714	First symmetric wing bending
10	2.754	2.769	2.935	3.415	2.752	3.265	First anti-symmetric wing bending
11	3.060	3.069	3.115	3.731	3.057	3.403	Symmetric tail bending
12	3.562	3.608	3.689	4.044	3.574	3.945	Forward fuselage lateral bending
13	4.440	4.449	4.511	4.790	4.429	4.602	First anti-symmetric tail bending
14	4.456	4.537	4.555	5.532	4.437	5.142	Second symmetric wing bending
15	4.818	4.842	5.146	5.832	4.809	5.542	Second anti-symmetric wing bending
16	5.449	5.465	5.550	6.158	5.444	5.994	Symmetric aft inner wing bending

Table 5. Buckling and strength analyses.

Analysis set	Gear configuration	Weight condition	Load cases
1	Up	DTOW	100, 200, 300, 600, 1100, 1200, 1300, 1400, & 1600
2	Up	ZFW	700, 800, 900, 1000, & 1700
3	Up	M2W	400 & 500
4	Down	DTOW	3001 ~ 3017 + 3018 ~ 3021 (emergency) + 1500 (for landing)
5	Down	DLW	4001 ~ 4017 + 4018 ~ 4021 (emergency) + 1800 (for landing)

Table 6. Minimum buckling load factor for baseline model before optimization from each analysis set.

Analysis set	Gear configuration	Weight condition	Case number	Load case	Minimum buckling load factor	Buckling
1	Up	DTOW	300	2.5G pull up; M=0.48	0.152	yes
2	Up	ZFW	1700	2.7G gust loads; M=0.89	0.195	yes
3	Up	M2W	400	2.5G pull up; M=2.00	0.151	yes
4	Down	DTOW	3006	Left one gear landing	1.71	no
5	Down	DLW	4006	Left one gear landing	1.52	no

Table 7. Minimum margins of safety for baseline model before optimization from each analysis set.

Analysis set	Gear configuration	Weight condition	Case number	Load case	Minimum margin of safety	Failure
1	Up	DTOW	1400	1.67G abrupt roll; M=0.48	-0.999	yes
2	Up	ZFW	1700	2.7G gust loads; M=0.89	-0.998	yes
3	Up	M2W	400	2.5G pull up; M=2.00	-0.997	yes
4	Down	DTOW	3013	Nose wheel yaw & steering (1)	-0.781	yes
5	Down	DLW	4003	Spring back landing	-0.657	yes

Table 8. Optimization histories of the first optimization run.

	Performance index		Design configuration	Before optimization	Iteration 1	Iteration 7
Objective function	Total weight		DTOW; GU	332738	425764	364105
Constraint functions $g_j(\mathbf{X})$	Flutter	$g_1(\mathbf{X})$	DTOW; GU; M=0.66	0.067(CV)	-0.362	-0.342
		$g_2(\mathbf{X})$	DTOW; GU; M=0.89	0.048(CV)	-0.543	**-0.096**
		$g_3(\mathbf{X})$	DTOW; GU; M=1.41	-0.079	-1.34	-0.297
		$g_4(\mathbf{X})$	FFEP; GU; M=0.66	0.066(CV)	-0.365	-0.337
		$g_5(\mathbf{X})$	FFEP; GU; M=0.89	0.034(CV)	-0.586	**-0.094**
		$g_6(\mathbf{X})$	FFEP; GU; M=1.41	-0.095	-1.32	-0.255
	Buckling	$g_7(\mathbf{X})$	DTOW; GU	0.152(CV)	-1.05	-1.29
		$g_8(\mathbf{X})$	ZFW; GU	0.186(CV)	-2.36	-3.09
		$g_9(\mathbf{X})$	M2W; GU	0.151(CV)	-1.28	-1.91
		$g_{10}(\mathbf{X})$	DTOW; GD	-0.960	-3.27	-3.88
		$g_{11}(\mathbf{X})$	DLW; GD	-0.561	-0.308	-1.07
	Strength	$g_{12}(\mathbf{X})$	DTOW; GU	**0.999(CV)**	-0.267	**-0.161**
		$g_{13}(\mathbf{X})$	ZFW; GU	0.998(CV)	-0.780	**-0.061**
		$g_{14}(\mathbf{X})$	M2W; GU	0.997(CV)	**-0.179**	-0.537
		$g_{15}(\mathbf{X})$	DTOW; GD	0.781(CV)	-0.751	**-5.63e-6**
		$g_{16}(\mathbf{X})$	DLW; GD	0.657(CV)	-0.210	-0.320

(CV): Constraint violated
GU: Gear up (retracted)
GD: Gear down (extended)
Iteration 2 through 6 not shown

Table 9. Summary of objective and constraint functions for the first and second optimization runs.

Functions	Performance indices	Notes
Objective (first run)	$F(\mathbf{X}) = (\mathrm{PI_W})^2 = W_T^2$	DTOW
Objective (second run)	$F(\mathbf{X}) = -\{0.5g_{12}(\mathbf{X}) + 0.5g_{13}(\mathbf{X}) + g_{15}(\mathbf{X})\}$	Safety factor = 1.5
Flutter constraint	$g_j(\mathbf{X}) = \mathrm{PI_F} = 1. - \frac{\mathrm{V_F}}{1.15\mathrm{V_L}} < 0. \quad \mathrm{j} = 1, 2, \ldots, 6$	15% margin
Buckling constraint	$g_j(\mathbf{X}) = \mathrm{PI_B} = (1/2)^2 - \{\text{positive min}(\mathrm{BLF}) - 1/2\}^2 < 0.$ $\mathrm{j} = 7, 8, \ldots, 11$	Safety factor = 1.5
Strength constraint	$g_j(\mathbf{X}) = \mathrm{PI_s} = -\min(\mathrm{MS}) < 0. \quad \mathrm{j} = 12, 13, \ldots, 16$	Safety factor = 1.5

Table 10. Optimization histories of the second optimization run.

	Performance index		Design configuration	Starting	BBBC 1	BBBC 2
Objective function	$-g_{12}(\mathbf{X})/2-g_{13}(\mathbf{X})/2-g_{15}(\mathbf{X})$			0.111	0.337	0.348
Constraint functions $g_j(\mathbf{X})$	Flutter	$g_1(\mathbf{X})$	DTOW; GU; M=0.66	-0.342	-0.342	-0.342
		$g_2(\mathbf{X})$	DTOW; GU; M=0.89	**-0.096**	**-0.096**	**-0.096**
		$g_3(\mathbf{X})$	DTOW; GU; M=1.41	-0.297	-0.297	-0.297
		$g_4(\mathbf{X})$	FFEP; GU; M=0.66	-0.337	-0.337	-0.337
		$g_5(\mathbf{X})$	FFEP; GU; M=0.89	**-0.094**	**-0.094**	**-0.094**
		$g_6(\mathbf{X})$	FFEP; GU; M=1.41	-0.255	-0.255	-0.255
	Buckling	$g_7(\mathbf{X})$	DTOW; GU	-1.29	-1.38	-1.38
		$g_8(\mathbf{X})$	ZFW; GU	-3.09	-3.09	-3.09
		$g_9(\mathbf{X})$	M2W; GU	-1.91	-2.23	-2.23
		$g_{10}(\mathbf{X})$	DTOW; GD	-3.88	-4.19	-4.19
		$g_{11}(\mathbf{X})$	DLW; GD	-1.07	-1.07	-1.07
	Strength	$g_{12}(\mathbf{X})$	DTOW; GU	**-0.161**	**-0.232**	**-0.232**
		$g_{13}(\mathbf{X})$	ZFW; GU	**-0.061**	**-0.145**	**-0.145**
		$g_{14}(\mathbf{X})$	M2W; GU	-0.537	-0.542	-0.542
		$g_{15}(\mathbf{X})$	DTOW; GD	**-5.63e-6**	**-0.159**	**-0.159**
		$g_{16}(\mathbf{X})$	DLW; GD	-0.320	-0.419	-0.419

(CV): Constraint violated
GU: Gear up (retracted)
GD: Gear down (extended)

Table 11. Design variable histories of the second optimization run.

Design variables	Starting	BBBC 1	BBBC 2
1 (2nd rib at inner-wing)	45°	15°	15°
2 (floor at main landing gear bay)	45°	65°	65°
3 (center wall at main landing gear bay)	45°	65°	55°
4 (aft bulkhead at main landing gear bay)	45°	65°	55°
5 (aft fuselage skin 1)	45°	30°	40°
6 (aft fuselage skin 2)	45°	50°	55°

Figures

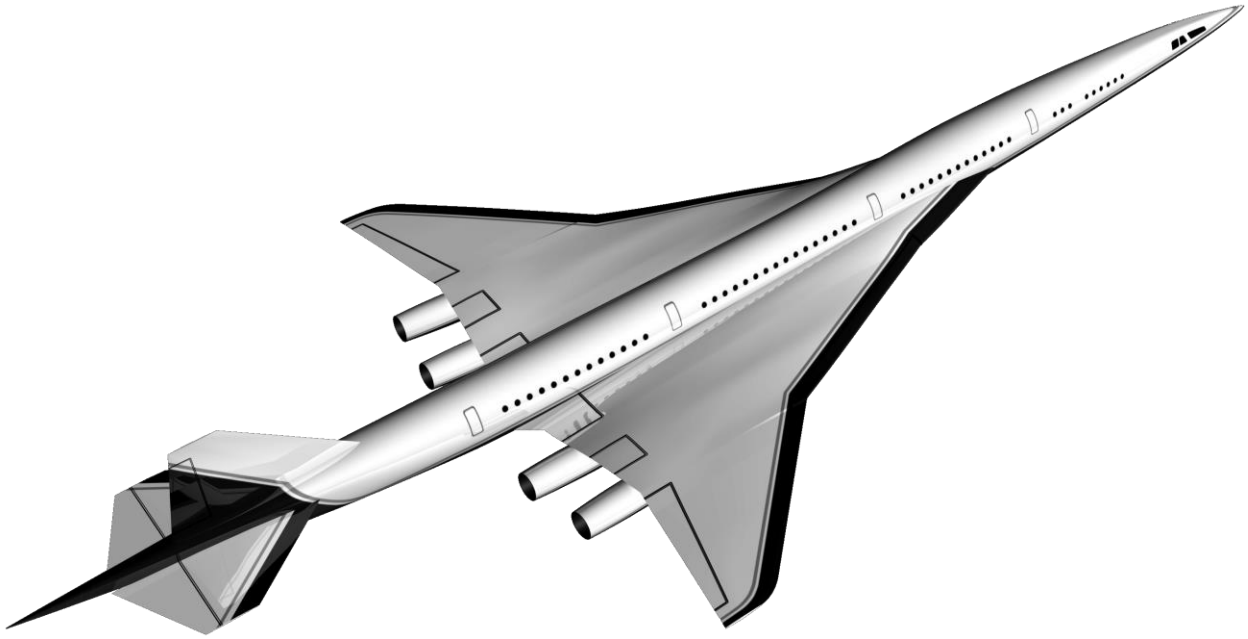

Figure 1. A high speed civil transport aircraft.

Figure 2. Artist's concept of the Lockheed Martin N+2 LSCT aircraft.

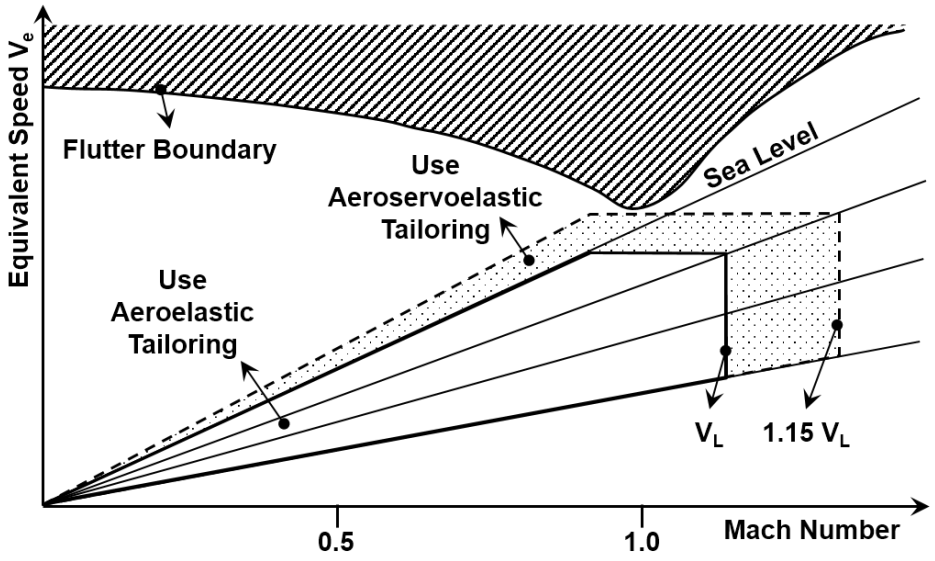

Figure 3. Aeroelastic stability envelope.

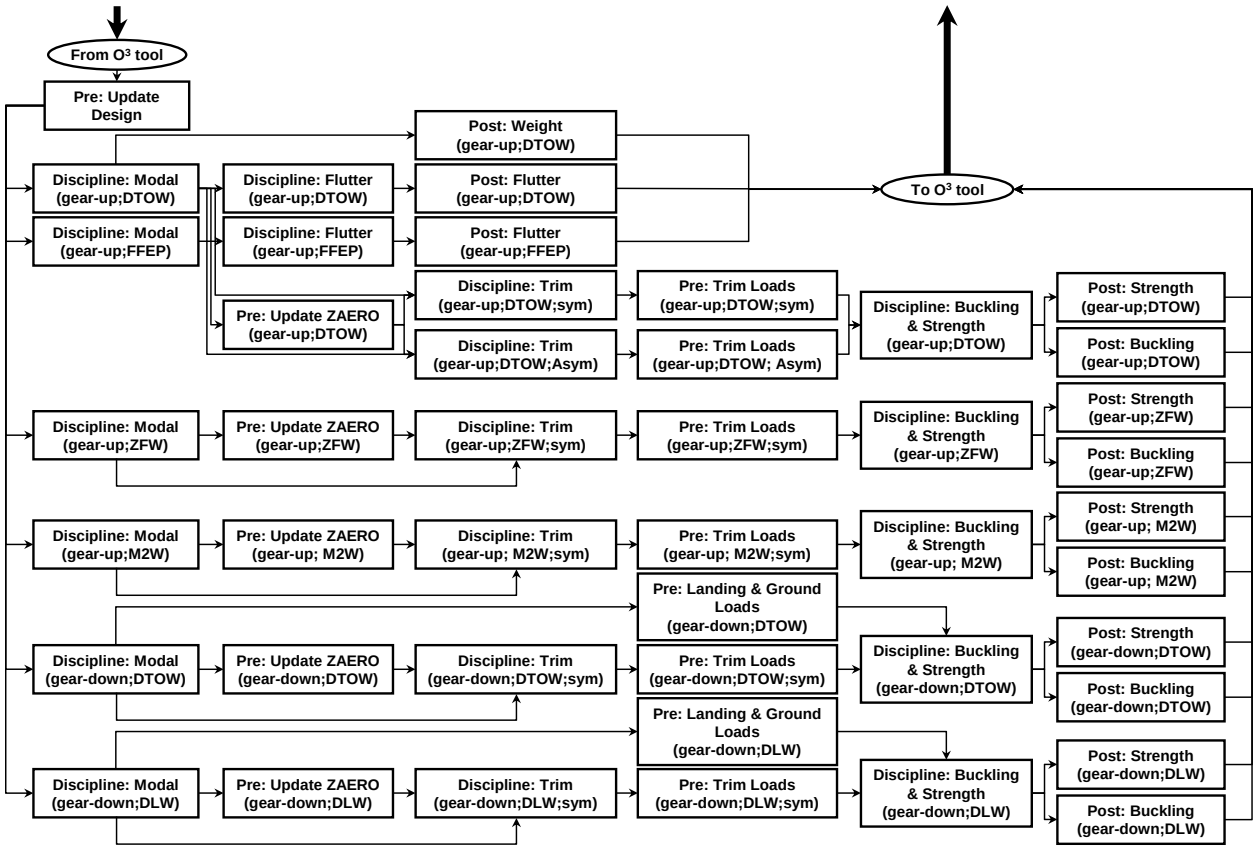

Figure 4. Details of pre-processor, discipline, and post-processor modules.

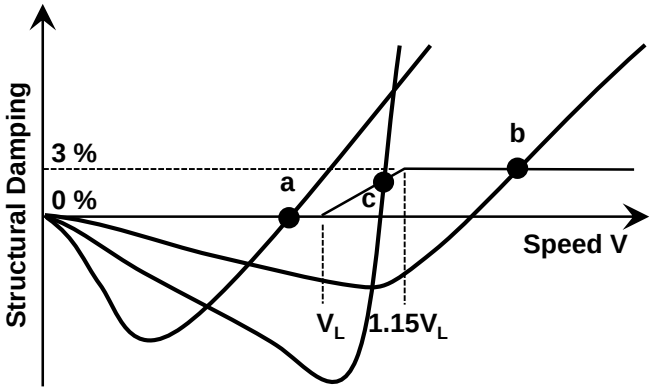

Figure 5. Definitions of flutter speed in three different speed regimes.

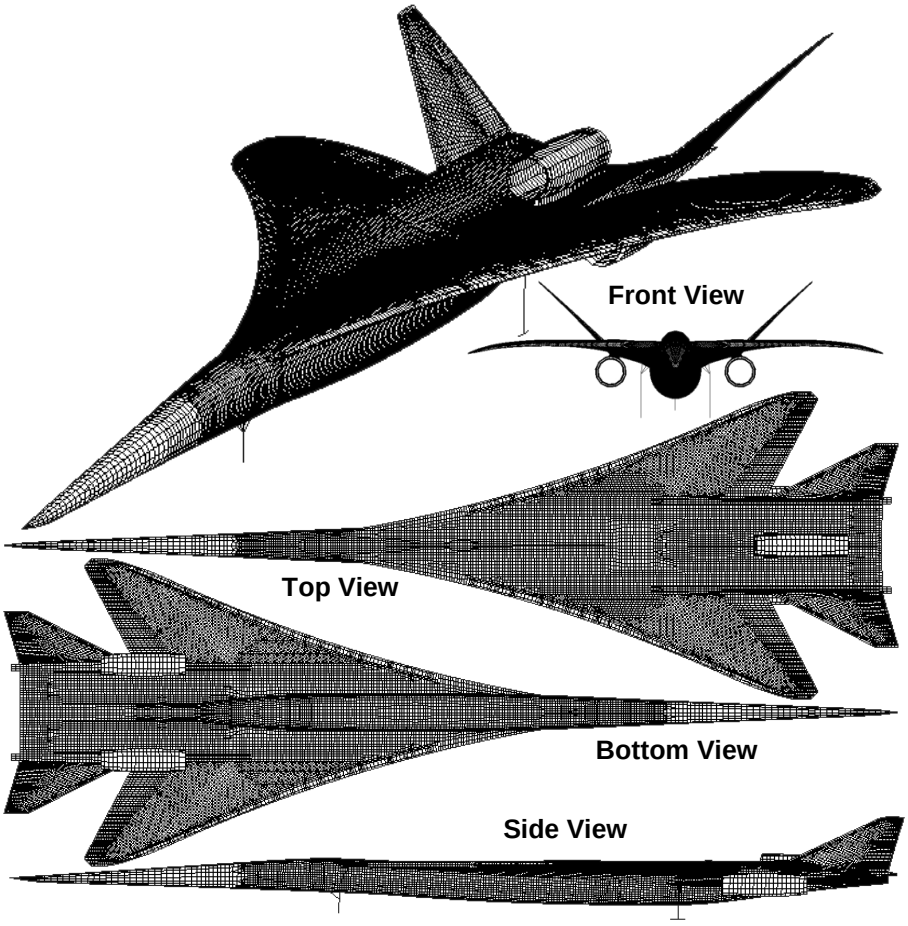

Figure 6. Finite element model of the N+2 LSCT aircraft in a gear-down configuration.

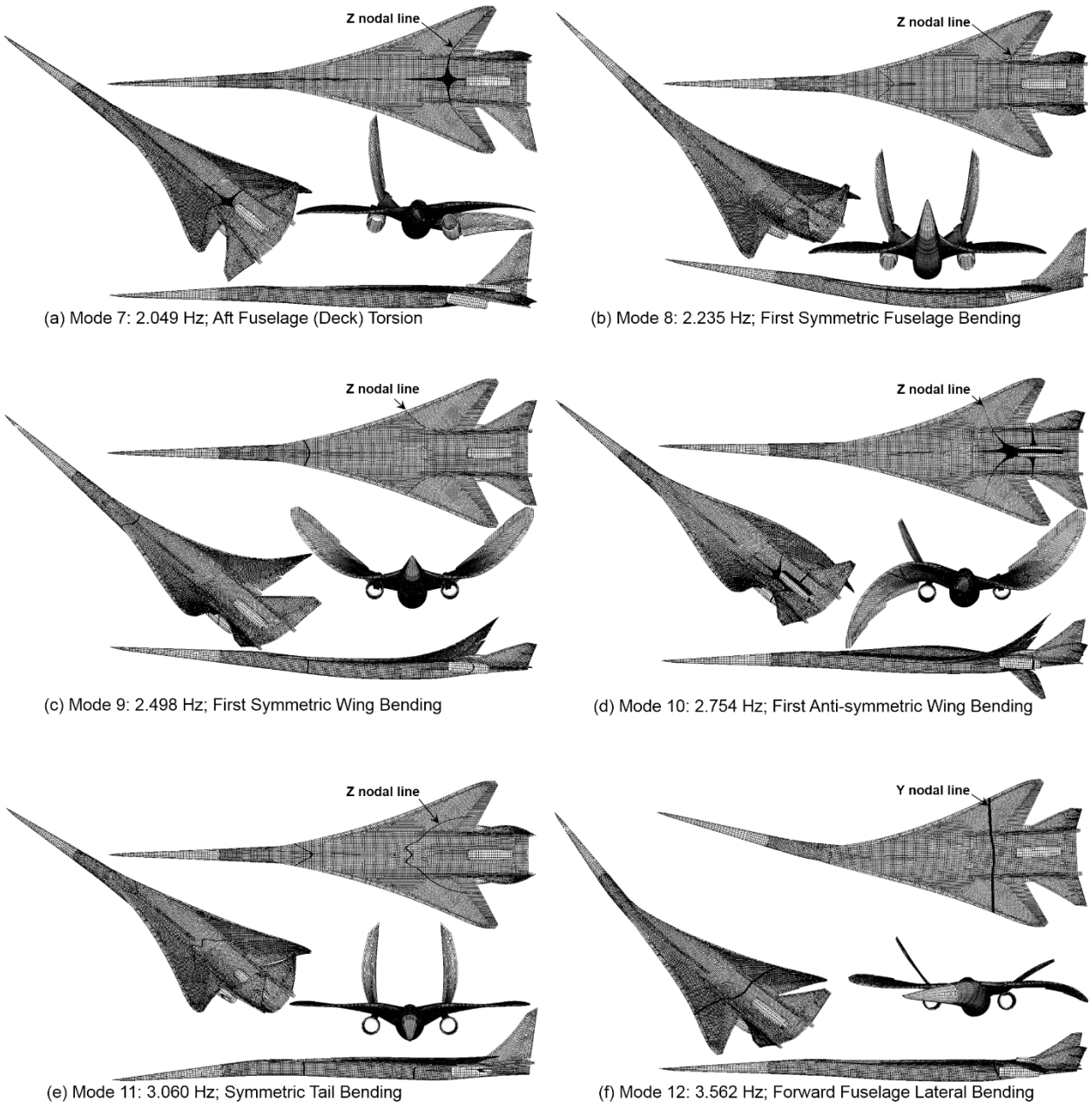

(a) Mode 7: 2.049 Hz; Aft Fuselage (Deck) Torsion

(b) Mode 8: 2.235 Hz; First Symmetric Fuselage Bending

(c) Mode 9: 2.498 Hz; First Symmetric Wing Bending

(d) Mode 10: 2.754 Hz; First Anti-symmetric Wing Bending

(e) Mode 11: 3.060 Hz; Symmetric Tail Bending

(f) Mode 12: 3.562 Hz; Forward Fuselage Lateral Bending

Figure 7. First six flexible mode shapes of the N+2 LSCT aircraft with a gear-up and DTOW weight configuration (before optimization).

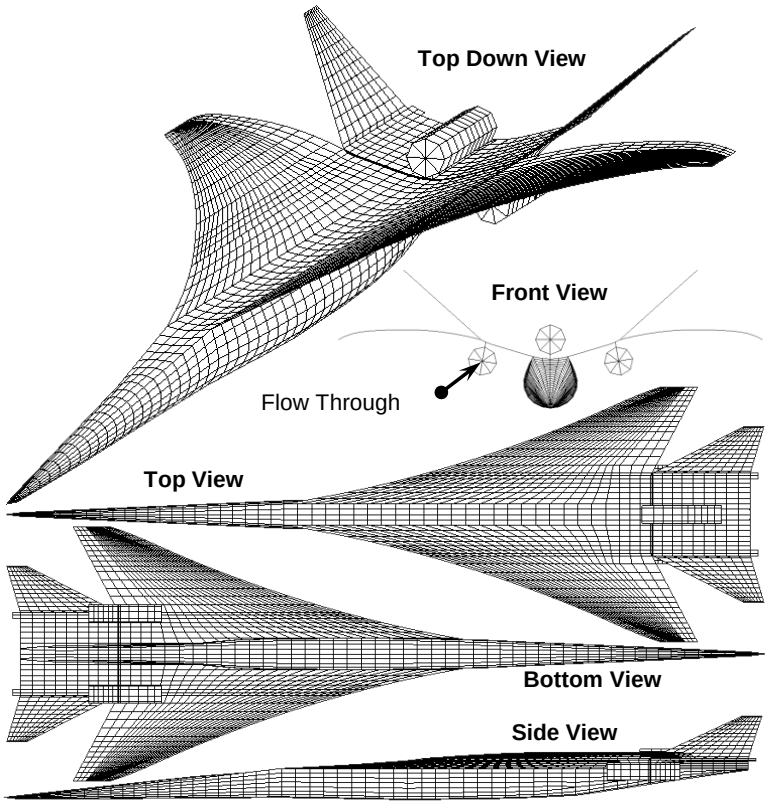

Figure 8. Aerodynamic model of the N+2 LSCT aircraft.

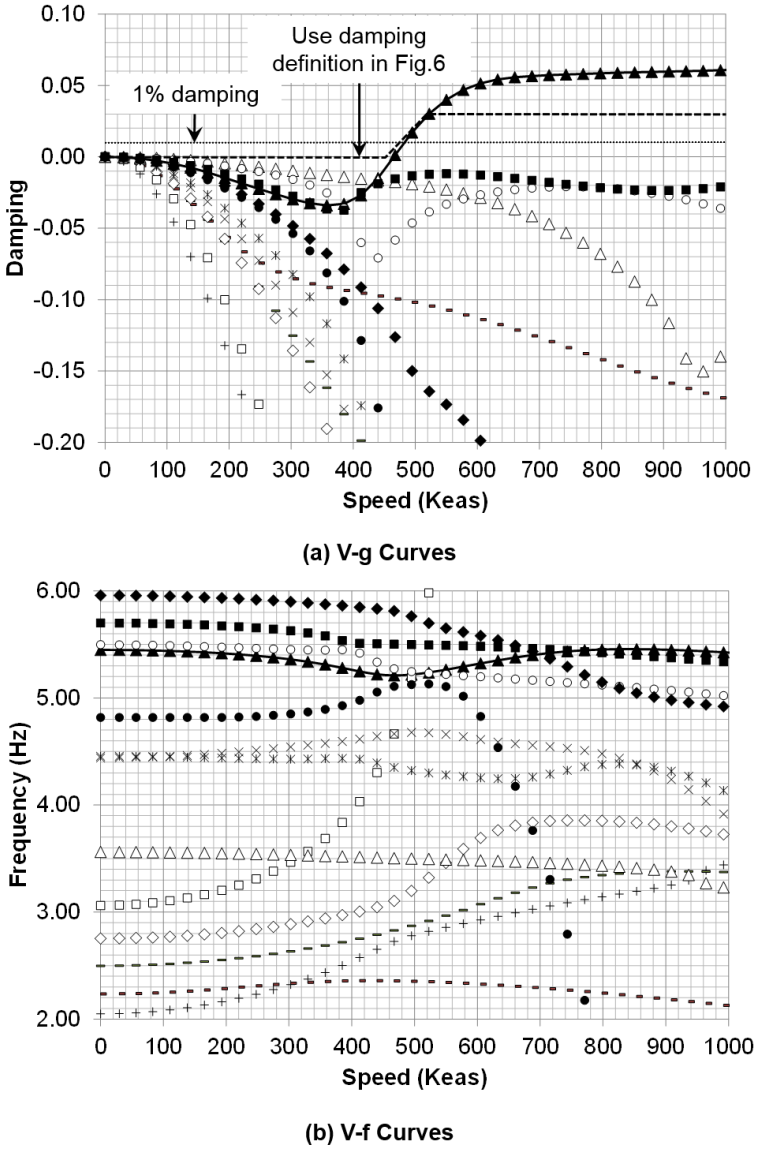

Figure 9. V-g and V-f curves of the N+2 LSCT aircraft with a gear-up and DTOW configuration at Mach 0.66 before optimization.

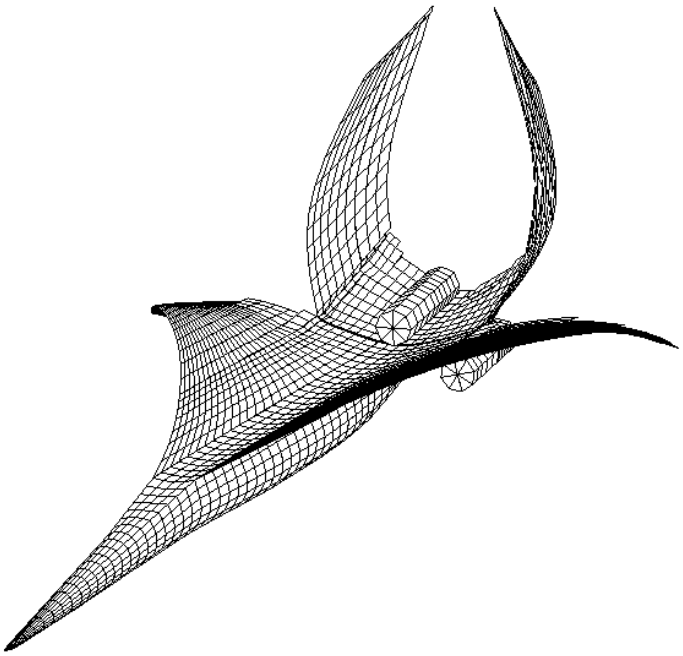

Figure 10. The primary flutter mode shape using the DTOW condition at Mach 0.66.

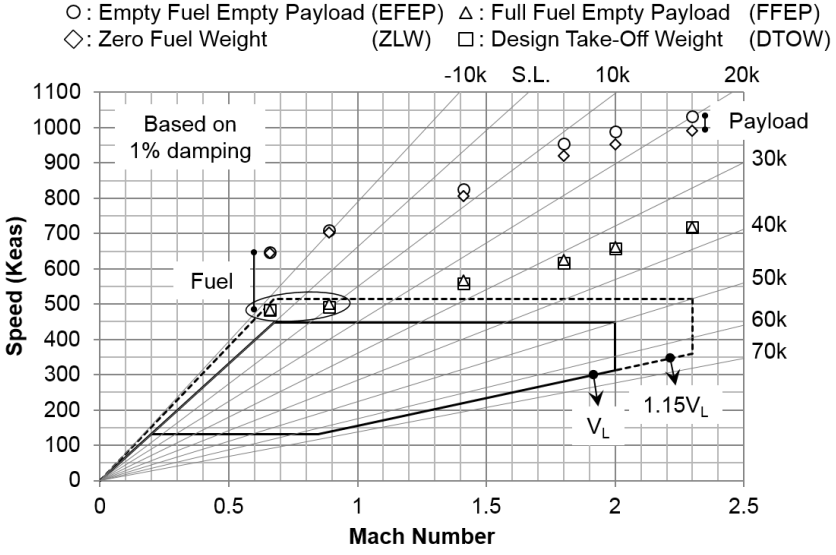

Figure 11. Flutter boundaries of the baseline N+2 LSCT aircraft before optimization.

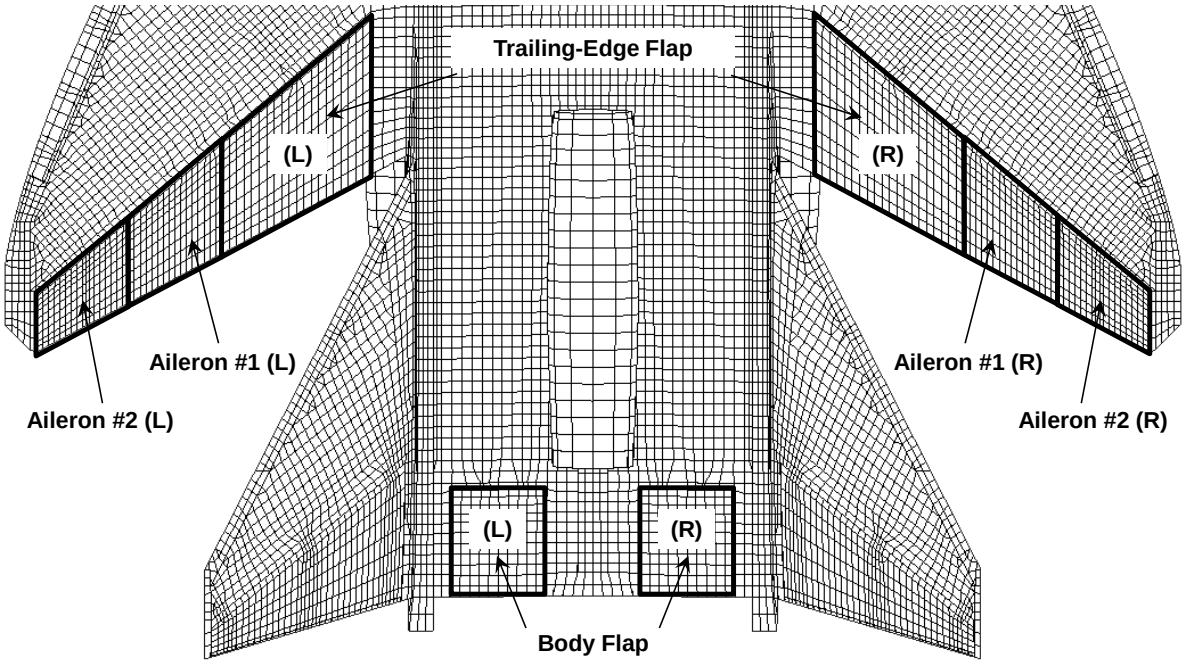

Figure 12. Control surfaces for trim analyses.

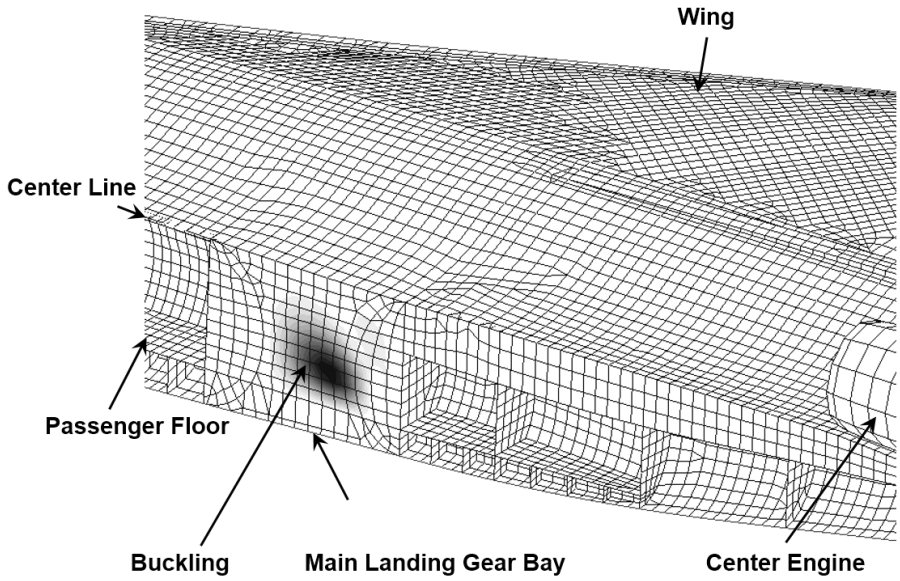

Figure 13. Buckling model shape under a 2.5g pull up maneuver at Mach 0.66 and sea level.

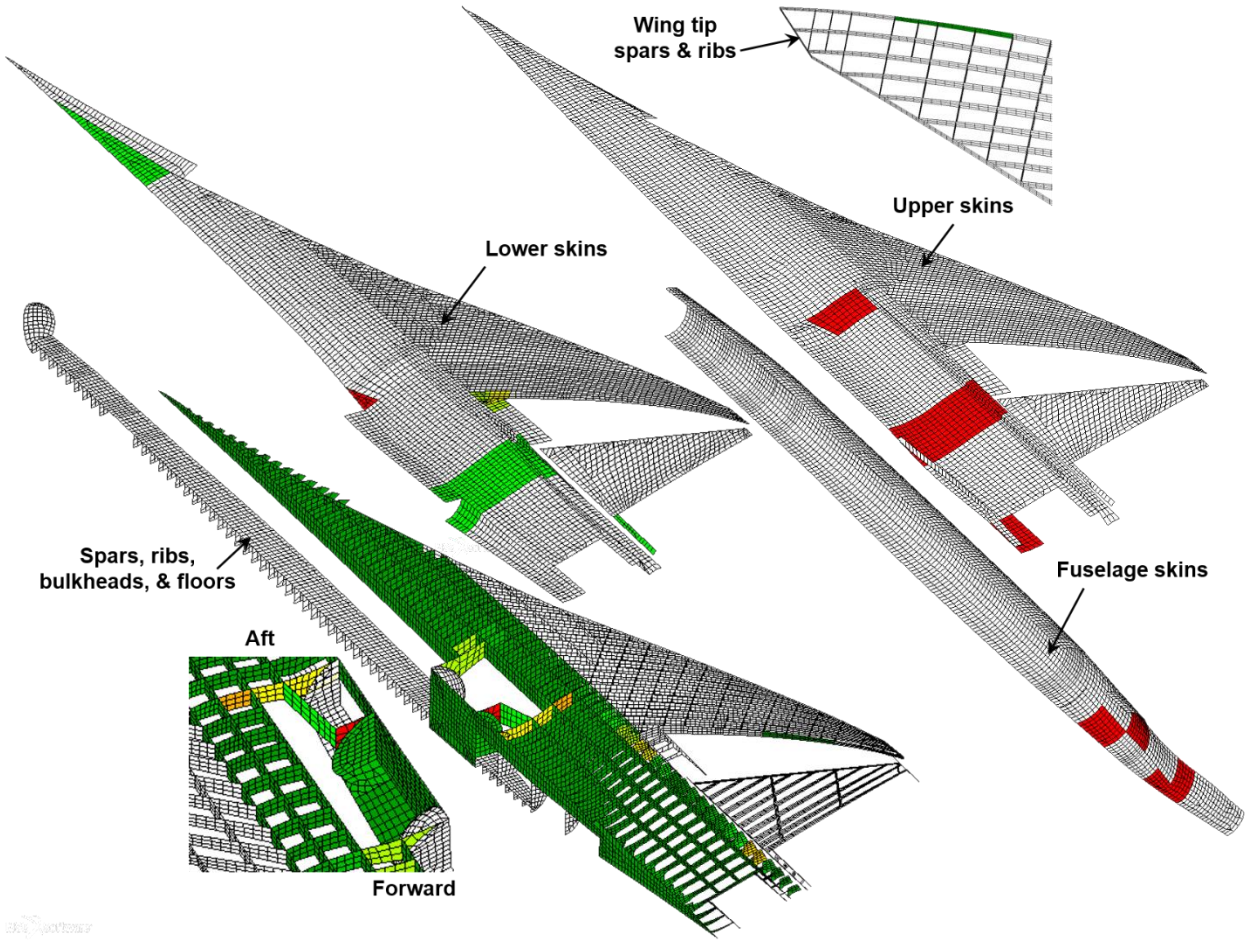

Figure 14. Structural components affected by thickness design variables.

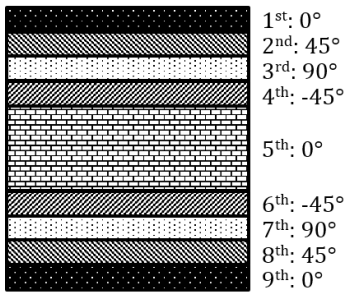

Figure 15. Symmetric stacking of nine plies into a composite laminate.

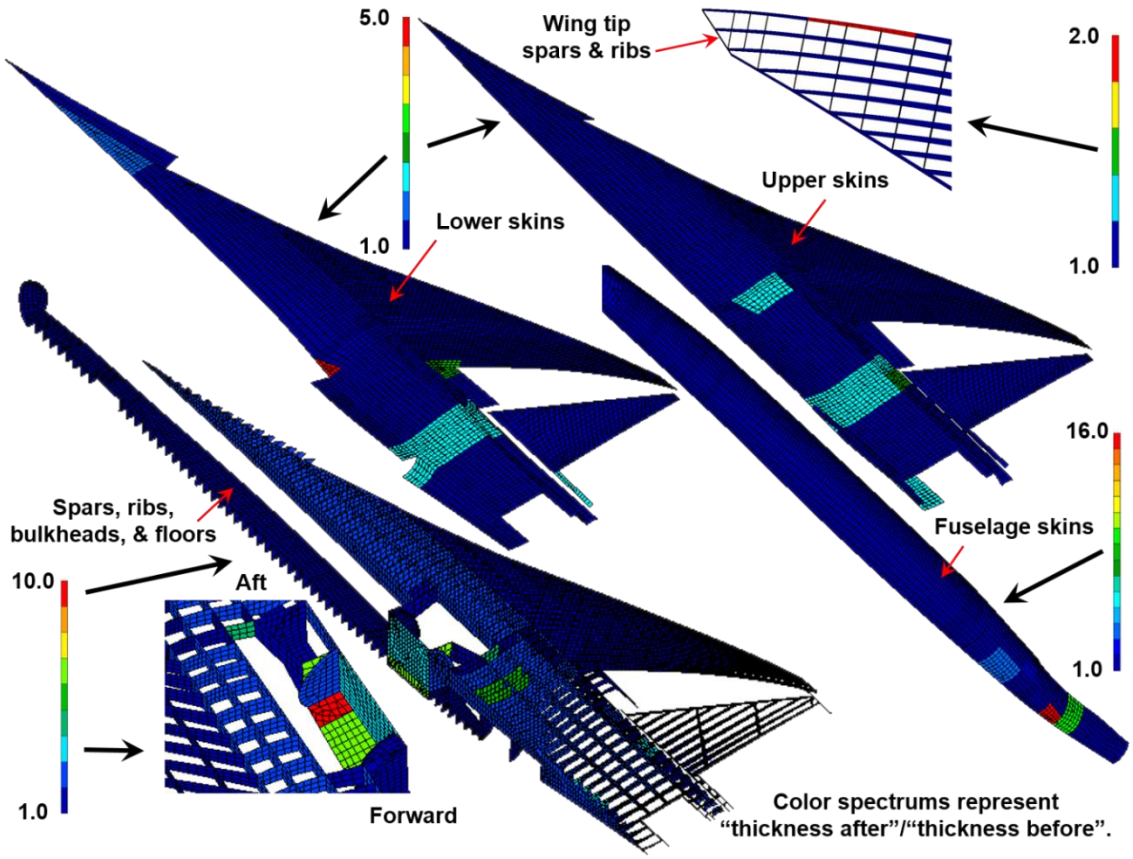

Figure 16. Thickness change of structural elements after iteration 7.

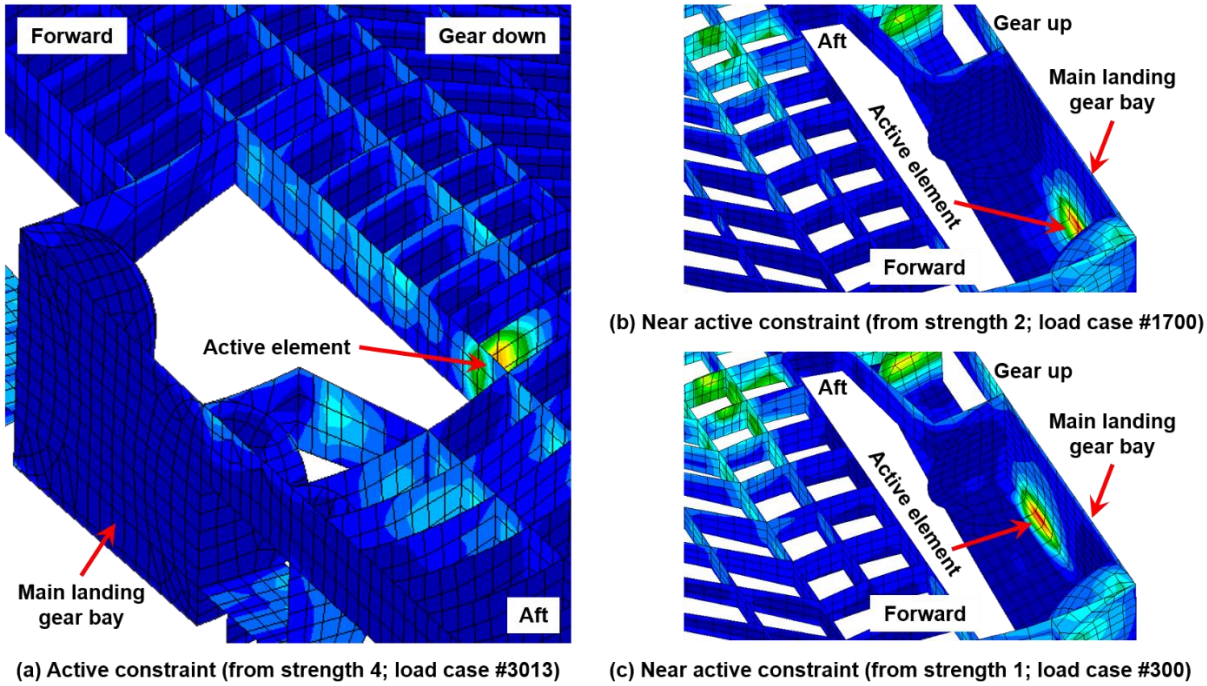

Figure 17. Strain distribution after iteration 7.

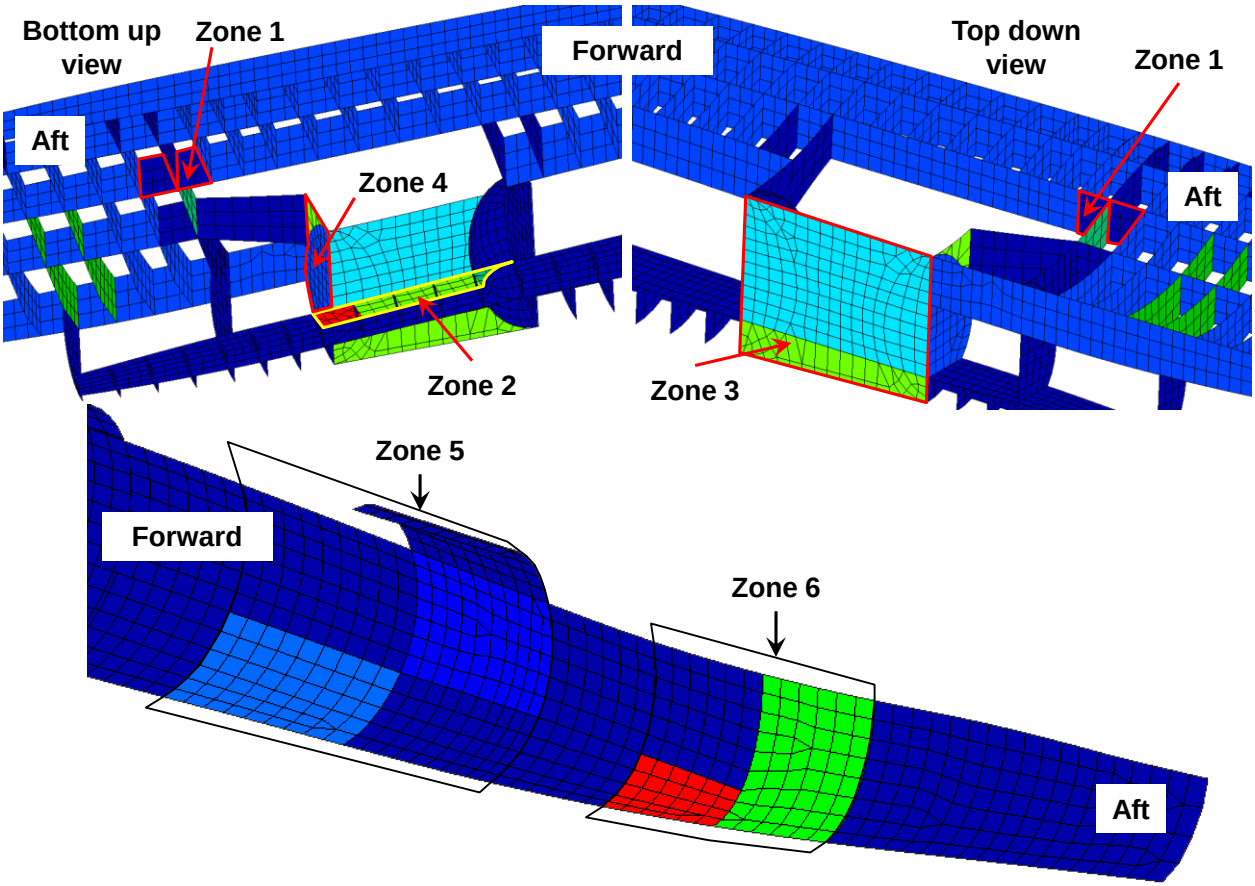

Figure 18. Design variable zones for composite ply angles.

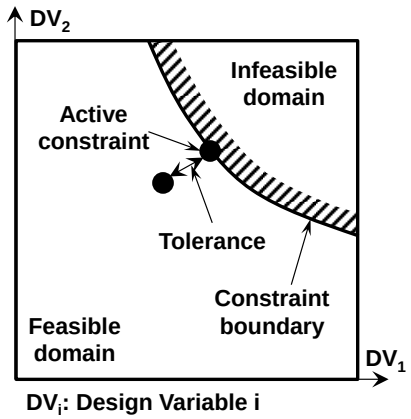

Figure 19. Definition of tolerance.

Appendix

Trim Results

In Table A1 (steady roll maneuver, load cases 1100 and 1300), roll rate in the trim card is defined in non-dimensional terms as equation (A1):

$$\frac{\mathrm{Pb}}{2V} = \frac{30°/sec \times \left(\frac{3.1416\ rad}{180°}\right) \times 83.89 ft \times 12\ in/ft}{2 \times (0.48 \times 13391.7\ in/sec)} = 0.0410\ rad \quad \text{(A1)}$$

In the case of an abrupt roll maneuver (load cases 1200 and 1400), roll acceleration is in units of rad/sec^2/g, since accelerations have been defined to be in units of g, and therefore equation (A2) is shown as:

$$\mathrm{Pdot} = 30°/sec^2 \times \left(\frac{3.1416\ rad}{180°}\right) \times 0.002588\ (\tfrac{1}{g}) = 0.0014 \frac{rad}{sec^2 \times g}. \quad \text{(A2)}$$

Table A1. Trim results.

Load case	100	200	300	400	500	600	700	800	900
Trim analysis	Symmetric								
Nx (g)	-0.007	-0.003	-0.005	0.001	0.002	-0.004	-0.016	-0.006	0.003
Nz (g)	2.5	-1.0	2.5	2.5	-1.0	2.5	2.5	-1.0	2.5
Pdot (rad/s^2/g)	None	None	None	None	None	None	None	None	None
Qdot (rad/s^2/g)	0.0	0.0	0.0	0.0	0.0	0.0	0.0	0.0	0.0
Pb/2V (rad)	None	None	None	None	None	None	None	None	None
Qc/2V (rad)	0.0	0.0	0.0	0.0	0.0	0.0	0.0	0.0	0.0
α (°)	7.75	-2.50	14.37	8.32	-2.81	16.90	4.10	-1.04	5.07
Body flap (°)	2.01	-6.07	6.12	-5.25	5.42	-25.68	-8.01	-1.59	-12.92
Trailing-edge flap (°)				-5.25		-25.68			-12.92
Aileron #1 (°)						-25.68			
Aileron #2 (°)						-25.68			
Mach number	0.66	0.66	0.48	2.00	2.00	1.41	0.66	0.66	2.00
Altitude (ft)	SL	SL	SL	49770	49770	49770	SL	SL	49770
Weight configuration	DTOW	DTOW	DTOW	M2W	M2W	DTOW	ZFW	ZFW	ZFW
Gear configuration	Up	Up	Up	Up	Up	Up	Up	Up	Up
Load case	1000	1100	1200	1300	1400	1500	1600	1700	1800
Trim analysis	Sym	Asymmetric (sym + anti-sym)				Symmetric			
Nx (g)	0.004	-0.002	-0.002	-0.004	-0.004	-0.002	0.002	-0.022	-0.001
Nz (g)	-1.0	0.0	0.0	1.67	1.67	1.0	1.0	2.7	1.0
Pdot (rad/s^2/g)	None	0.0	0.0014	0.0	0.0014	None	None	None	None
Qdot (rad/s^2/g)	0.0	0.0	0.0	0.0	0.0	0.0	0.0	0.0	0.0
Pb/2V (rad)	None	0.0410	0.0	0.0410	0.0	None	None	None	None
Qc/2V (rad)	0.0	0.0	0.0	0.0	0.0	0.0	0.0	0.0	0.0
α (°)	-1.44	0.40	0.40	9.74	9.74	13.91	6.02	4.95	9.07
Body flap (°)	11.89	-2.86	-2.86	3.14	3.14	8.00	-9.87	-13.20	22.52
Trailing-edge flap (°)							-9.87		
Aileron #1 (°)		19.07	48.63	19.07	48.63				
Aileron #2 (°)		19.07	48.63	19.07	48.63				
Mach number	2.00	0.48	0.48	0.48	0.48	0.3092	1.80	0.89	0.3092
Altitude (ft)	49770	SL	SL	SL	SL	SL	55000	20000	SL
Weight configuration	ZFW	DTOW	DTOW	DTOW	DTOW	DTOW	DTOW	ZFW	DLW
Gear configuration	Up	Up	Up	Up	Up	Down	Up	Up	Down

References

[1]Bhatia, K. G., and Wertheimer, J., "Aeroelastic Challenges for a High Speed Civil Transport," AIAA-93-1478-CP, 1993.

[2]Pak, C.-G., and Goggin, P. J., "Automated Matched Flutter Optimization of the HSCT Aircraft," *Computer Modeling and Simulation in Engineering*, Vol 2, 1996, pp. 203-221.

[3]Locatelli, D., Liu, Q., Tamijani, A. Y., Mulani, S. B., and Kapania, R. K., "Multidisciplinary Optimization of Supersonic Wing Structures Using Curvilinear Spars and Ribs (SpaRibs)," AIAA 2013-1931, 2013.

[4]Lukaczyk, T., Palacios, F., and Alonso, J. J., "Response Surface Methodologies for Low-Boom Supersonic Aircraft Design using Equivalent Area Distributions," AIAA 2012-5705, 2012.

[5]Silva, W. A., De La Garza, A., Zink, S., Bounajem, E. G., Johnson, J. C., and et.al, "The NASA High Speed ASE Project: Computational Analyses of a Low-Boom Supersonic Conguration," AIAA 2014-0675, 2014.

[6]*MSC/NASTRAN 2005 Quick Reference Guide*, The MacNeal-Schwendler Corporation, Newport Beach, California, 2005.

[7]Li, W. W., and Pak, C.-G., "Aeroelastic Optimization Study Based on the X-56A Model," AIAA-2014-2052, 2014.

[8]Livne, E., Schmit, L. A., and Friedmann, P. P., "An Integrated Approach to the Optimum Design of Actively Controlled Composite Wings," AIAA-89-1268, 1989.

[9]Livne, E., Schmit, L. A., and Friedmann, P. P., "Exploratory Design Studies Using an Integrated Multidisciplinary Synthesis Capability for Actively Controlled Composite Wings," AIAA-90-0953, 1990.

[10]*ZAERO User's Manual Version 8.5*, ZONA Technology, Inc., Scottsdale, Arizona, 2011.

[11]Pak, C.-G., "Preliminary Development of an Object-Oriented Optimization Tool," NASA/TM-2011-216419, 2011.

[12]Federal Aviation Regulations, "Airworthiness Standards: Transport Category Airplanes," Part 25, Federal Aviation Administration, 1993.

[13]Vanderplaats, G. N., "ADS – A Fortran Program for Automated Design Synthesis, Ver. 1.10," NASA CR-177985, 1985.

[14]*DOT Design Optimization Tools User's Manual Version 5.0*, Vanderplaats Research & Development, Inc., Colorado Springs, Colorado, 1999.

[15]Erol, O. K., and Ibrahim E., "A New Optimization Method: Big Bang-Big Crunch," *Advances in Engineering Software*, Vol. 37, No. 2, 2006, pp. 106–111.

[16]Camp, C. V., "Design of Space Trusses Using Big Bang-Big Crunch Optimization," *Journal of Structural Engineering*, Vol. 133, No. 7, 2007, pp. 999-1008.

[17]Kaveh, A., and Talatahari, S., "Size Optimization of Space Trusses Using Big Bang-Big Crunch Algorithm," *Computers and Structures*, Vol. 87, No. 17-18, 2009, pp. 1129–1140.

[18]Pak, C.-G., and Truong, S. S., "Extension of an Object-Oriented Optimization Tool: User's Reference Manual," NASA/TM-2015-218733, 2015.